Surface Charge Driven Growth of Eight-branched Cu_2O Crystals

Katherine Self and Wuzong Zhou*

EaStChem, School of Chemistry, University of St Andrews, St Andrews, KY16 9ST, United Kingdom.

ABSTRACT: Cu_2O crystals are synthesised hydrothermally with an 8-branched morphology, which can undergo a transition to a cubic shape by increasing the reaction time. The rapid branch formation of these structures is studied over time using SEM, TEM, SAED, PXRD and TGA. The formation of Cu^{2+}/PVP soft matter clusters is shown to play a key role in the reduction of Cu^{2+}, the nucleation of Cu_2O crystals and the rapid growth of branches along all eight equivalent <111> directions of the cubic Cu_2O structure, due to the presence of negatively charged hydroxyl sites on the {111} surfaces. This non-classical crystal growth mechanism, which relies on aggregation of the precursor on the crystal surface, may help us to understand the formation of many abnormal crystal morphologies.

INTRODUCTION

Cuprous oxide, Cu_2O, is a semiconductor material which has a cubic structure, a direct band gap of 2.137 eV [1,2] and which typically exhibits p-type semiconductor characteristics due to the presence of Cu vacancies.[3-5] Due to its unique and interesting magnetic and optical properties, Cu_2O has been widely studied due to its potential applications in a huge range of fields such as catalysis,[6,7] gas sensing [8] and the conversion of solar energy into chemical or electrical energy [9-11] as well as having been at the centre of research into the Bose-Einstein condensation of excitons.[12]

Cu_2O has been shown to exhibit a wide variety of morphologies such as thin films,[13,14] nanorod arrays,[15] nanospheres or nanocubes [16-18] and even hollow crystals.[19,20] Since the suitability of Cu_2O for its various applications is so highly dependent on its morphology and microstructure,[21] an array of different and often complicated techniques have been utilised to attempt to control the shapes and sizes of Cu_2O crystals. These have included electrochemical deposition,[22-25] high pressure sputtering,[26] sonochemical methods [27] and many other techniques [28,29] but the control of Cu_2O morphologies synthesized via more facile, hydrothermal routes has rarely been reported.

More recently, there has been interest in dendritic or branched morphologies and, in particular, the highly symmetric "8-pod branching growth" [30-32] of Cu_2O crystals as the high degree of branching in such structures results in a much higher surface area than that of the more typical cubic or octahedral Cu_2O crystals and may, therefore, increase the efficiencies of Cu_2O crystals for their various applications. Little is understood about the mechanism by which these structures form, however, as many highly symmetric metal oxide crystals are thought to be single crystals so their growth goes unstudied as they are assumed to follow the classical growth route, first established over 100 years ago. This so-called "bottom-up" theory of crystal growth is described by the Bravais-Friedel-Donnay-Harker (BFDH) law [33-35] and Hartman-Perdok theory [36] and explains how single crystals are formed from a single nucleus via layer-by-layer deposition of the building units on the crystal surfaces.

In the present work, a simple hydrothermal synthesis is presented to form Cu_2O crystals with an 8-branched morphology, which then undergo a transition to a cubic shape. By analysing the time-dependent growth of these particles, we present evidence that the classical theories cannot explain the rapid growth of branches along the <111> zone axes and show that, instead, the organic agents added to the solution disturb the environment for free crystal growth, leading to a new, non-classical mechanism. Detailed studies of the surface structures of the principal terminating facets of Cu_2O will also be described, revealing that the unique surface charge of the terminating {111} facets is crucial to the rapid branch growth along the <111> zone axes.

EXPERIMENTAL SECTION

Sample preparation. The synthetic procedure used in this work was adapted from that reported by Guo *et al*.[16] for the generation of Cu_2O crossed nanocubes. Firstly, 0.17 g copper (II) chloride dihydrate was dissolved in 5 ml distilled water and, separately, 0.2 g polyvinylpyrrolidone (PVP) (Mw ~ 55,000) was dissolved into 5 ml distilled water. The two solutions were added to 55 ml distilled water forming a pale blue solution that was then stirred for 30 min.

In the next step, 0.69 g potassium carbonate and 0.64 g monosodium citrate were dissolved in 10 ml distilled water. This solution was then added to the light blue aqueous solution from the first stage, which instantly turned to a much darker blue colour. Next, 0.9 g D-glucose was dissolved in 5 ml distilled water and then added to the dark blue solution.

The final solution was stirred for a further 10 min and then 35 ml of it was transferred to a 50 ml Teflon-lined autoclave which was sealed and heated in an oven at 80 °C for different reaction times of 1.5, 2, 4, and 13 h as well as one much longer time of 20 days. The resulting precipitate was collected after each reaction via centrifugation, washed with ethanol and distilled water and dried over night at 40 °C. To confirm the roles of organic compounds, experiments were also performed (1) with the glucose removed from the synthesis over 4 h, and (2) with PVP removed from the synthesis system.

Sample characterization. Scanning electron microscopy (SEM) was performed on the samples via the use of a Jeol-JSM-6700F field-emission gun microscope, operated between 1 to 5 kV in gentle mode. In order to avoid beam charging, each sample was coated with a thin film of gold prior to being inserted into the microscope column. Transmission electron microscopy (TEM), high resolution TEM (HRTEM) and selected area electron diffraction (SAED) were performed through the use of a JEOL JEM-2011 electron microscope, operated at an accelerating voltage of 200 kV and fitted with a LaB_6 filament. For these

experiments, each powder sample was ground in acetone with a pestle and mortar and then deposited dropwise onto a grid coated with a holey carbon film. The images were recorded using a Gatan 794 CCD camera. Energy dispersive X-ray spectroscopy (EDS) was performed to detect the composition of the samples using an Oxford INCA system attached to Joel JSM-6700F microscope, when an accelerate voltage of 20 kV was applied. Powder X-ray diffraction (PXRD) patterns were obtained using a PANalytical Empyrean diffractometer, with Cu K_α radiation (λ = 1.5418 Å). Highscore Plus software was used to analyse the resulting PXRD patterns. Thermal gravimetric analysis (TGA) was carried out using a Stanton Redcroft STA-780 series instrument. 15 - 20 mg of the dry powders was heated in a constant flow of air at a ramp rate of 2 °C per min from room temperature to 600 °C, held for 2 h and then cooled to room temperature at a rate of –5 °C per min.

RESULTS AND DISCUSSION

Cuprous oxide, Cu_2O, crystals synthesised over a range of growth times were first analysed via SEM (**Figure 1**). This revealed variations in the morphology of the crystals, which started as 8-branched particles at the earliest growth time of 1.5 h (**Figure 1a**), with the branches appearing to grow along the <111> directions of a cubic core. By a reaction time of 2 h, the dominant growth direction had become <100>, i.e. the branches had grown thicker, showing four diamond figures on the (100) projection, as the morphology appeared to transition towards a cubic shape (**Figure 1b**). The space between the branches became smaller and smaller over time until all eight branches were connected (**Figure 1c**) and then the space between them filled out, with increased growth on the {100} faces until finally, after 13 h, all the Cu_2O crystals appeared as cubes (**Figure 1d**). EDS results from these particles showed only C, O, and Cu. Low magnification SEM images of the samples with different growth times shown in **Figure S1** in Supporting Information (SI) confirm that these morphologies are typical in the samples during the crystal growth, although at early stages, the morphologies of the particles are not uniform.

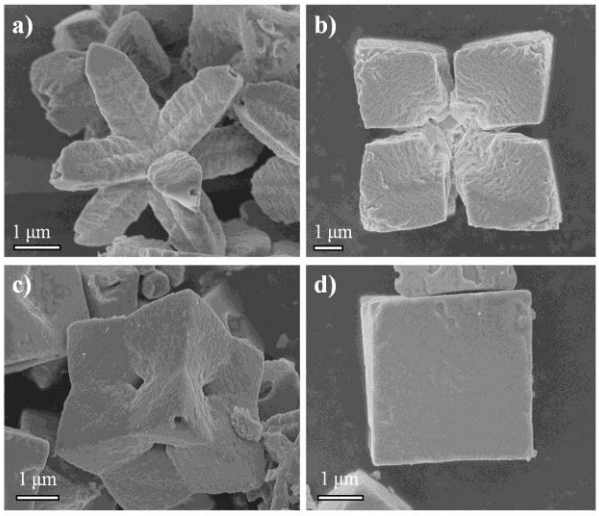

Figure 1. SEM images displaying the typical morphologies observed of Cu_2O crystals grown over a) 1.5 h, b) 2 h, c) 4 h and d) 13 h.

In order to study this interesting morphology evolution in more detail, PXRD analysis was also carried out on the samples over a range of growth times. As shown in **Figure 2**, crystalline Cu_2O had formed very rapidly and so could be observed from the earliest growth time tested of 2 h onwards. The yield from the 1.5 h experiment was so low that there was insufficient sample for PXRD testing. The peaks in **Figure 2** marked ● have been indexed to the cubic Cu_2O phase with unit cell parameter a = 4.2797 Å and space group $Pn\bar{3}m$. The intensity ratios of the peaks in the patterns in **Figures 2a** and **2c** are similar to those observed from common powders of Cu_2O (PDF card no: 01-075-6237). However, the relative intensity of the (200) peak increases significantly in the 4 h sample (**Figure 2b**). This unusual phenomenon implies that during the morphology evolution from the 8-branched particles to cubic particles, the dominant crystal growth direction is along the <100> zone axes.

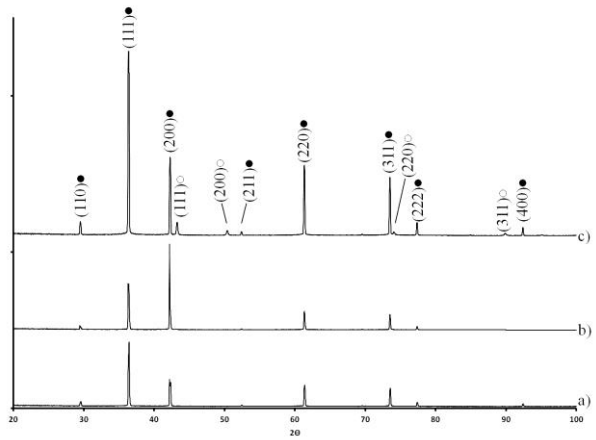

Figure 2. PXRD patterns of samples grown over a) 2 h, b) 4 h and c) 13 h. The peaks marked ● have been indexed to cubic Cu_2O and those marked ○ are indexed to cubic Cu.

The PXRD pattern from the sample grown over 13 h (**Figure 2c**) revealed a few low intensity peaks that could not be indexed to Cu_2O but which actually represent the cubic Cu metal phase. These peaks have been marked ○ and are indexed to cubic Cu with unit cell parameter a = 3.6200 Å and space group $Fm\bar{3}m$.

TEM images, HRTEM images and SAED patterns were recorded from the branched particles to determine the microstructure of the early stage sample grown over 2 h (**Figure 3**). Although the particles contained some organic components as indicated by the presence of carbon peak in the EDS spectra and by the TGA results discussed below, the samples were quite stable under the electron beam irradiation when the electron dose was not too high.[37] Both single-crystal-like and polycrystalline-like SAED patterns were observed as shown in the insets in **Figures 3a** and **3c**, respectively. The HRTEM image in **Figure 3b** shows many crystalline domains that appear fairly well aligned (hence the corresponding single-crystal-like diffraction pattern) despite being separated by some amorphous matter as indicated by the arrow. The measured d-spacings marked A (2.44 Å) and B (2.12 Å) can be indexed to the (111) and (200) planes of cubic Cu_2O, respectively.

In contrast, the HRTEM image in **Figure 3d**, shows many unaligned crystalline nanodomains, resulting in the corresponding polycrystalline-like SAED pattern. The lattice fringes could still be indexed to Cu_2O with the d-spacing labelled C measuring 1.73 Å and D measuring 1.14 Å, corresponding to the (211) and (321) planes of cubic Cu_2O, respectively.

Since the 8-branched particles had been broken for HRTEM imaging, the original locations of the fragments observed in TEM and HRTEM cannot be recovered. However, although both of the particles in **Figure 3** are actually polycrystalline, the former has an obviously higher crystallinity. Star-shaped particles with multiple branches [38,39] and spherulite particles [40,41] with high density needles have been previously reported. However, the branches and needles in these particles have no specific relationship, unlike the particles observed in the present work, where 8 branches growing perfectly along all the <111> directions of a cubic structure. We therefore hypothesize that, in an 8-branched particle, the central particle should have a higher crystallinity than that in the branches. This is why the 8 {111} faces are well orientated. The particle in **Figure 3a** is, therefore, likely to be from a central seed particle, which ideally has an octahedral shape with 8 {111} facets of the cubic Cu_2O.

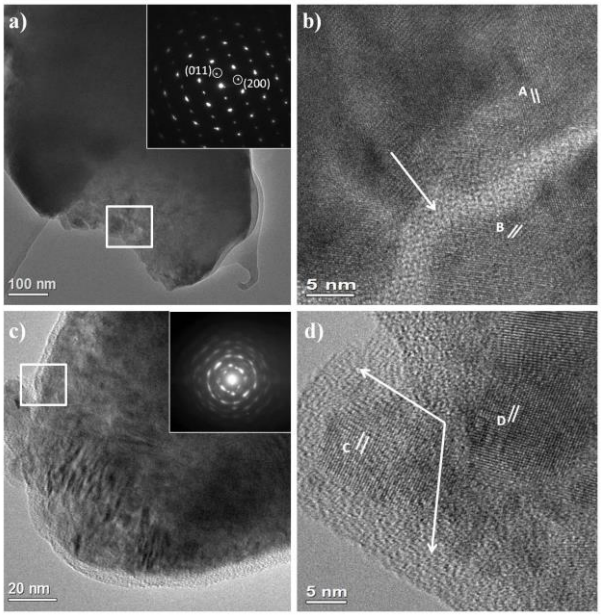

Figure 3. TEM analysis of the 2 h sample. a) TEM image with corresponding, single-crystal-like diffraction pattern inset. b) HRTEM image from the area marked with a square in a). c) TEM image with corresponding, polycrystalline-like diffraction pattern inset. d) HRTEM image from the area marked with a square in c). The *d*-spacings marked A, B, C and D measure 2.44 Å, 2.12 Å, 1.73 Å and 1.14 Å, which can be indexed to the (111), (200), (211) and (321) planes of Cu_2O, respectively. The arrows in b) and d) indicate the amorphous organic component present.

In order to find more evidence of this seed particle to support this hypothesis, the 1.5 h sample was lightly crushed and analysed again via SEM. The size of the seed particles was revealed to be approximately 1.5 μm. Four {111} facets, which belong to the top half of an octahedron are clearly seen in **Figure S2b** in SI, after four branches are removed. The combination of these SEM images and the single crystal domains identified via HRTEM go some way to support the proposition of a seed crystal from which the branches grow outwards. On the other hand, the shape of the particle in **Figure 3c** looks like a tip of a branch where some nanocrystallites have developed in an amorphous matrix, but they are randomly orientated.

As indicated by the arrows in **Figure 3**, it is clear that there is an amorphous, more likely organic, component present in the 2 h sample in which the Cu_2O nanocrystallites are embedded. TGA analysis was carried out to confirm the existence of an organic component within the particles. This analysis is displayed in **Figure S3** in SI, where it can be seen that the amount of this organic component decreases as the growth time is extended from 2 h to 13 h.

The organic polymer, PVP, which was stirred thoroughly into the copper solution, would play a key role in the early crystal growth stages as it can interact strongly with Cu^{2+} ions in aqueous solution, causing them to aggregate together. Shahmiri *et al*.[14] reported the use of PVP to synthesise PVP-coated copper oxide, CuO, nanosheets via a quick precipitation method for use as antibacterial and antifungal agents. In their mechanism, a Cu^{2+}/PVP matrix formed rapidly as an intermediate step in the formation of CuO.

PVP is composed of a polyvinyl skeleton with polar amide groups, which are able to donate hydrogen bonds on both the O and N. It has the potential, therefore, to form coordinative bonds with Cu^{2+} cations, resulting in a complex, denoted Cu^{2+}/PVP. In this way, PVP has been used to act as a stabiliser for metal salts dissolved in aqueous solution through the electrostatic stabilisation of the amide groups of the pyrrolidone rings.[42] In the present work, the Cu^{2+} precursor forms a Cu^{2+}/PVP cluster according to the same mechanism. Harada and Fujiwara have also reported the formation of a Cu^{2+}/PVP matrix [43] and go further; explaining that as the interaction between the metallic ions and the PVP molecules allows the metallic ions to gather so closely together, PVP can in fact be used as an agent for the formation of rod-like metal particles that form along the linear PVP backbone. A parallel experiment was performed using the same synthetic system without adding PVP. It was found that the growth of Cu_2O crystals was much lower and 8-branched particles were not observed.

A buffer solution with a pH value of 7 containing potassium carbonate and monosodium citrate was added during the synthesis, resulting in the solution instantly turning a darker, more intense blue. This addition did not only maintain the neutral conditions of the solution and further condense Cu^{2+} in the Cu^{2+}/PVP clusters, but also lead to hydroxylation of Cu^{2+} as the citrate ions are able to pull protons from water molecules, causing the release of OH^- ions from the surrounding solution that rapidly combine with Cu^{2+} cations.[44] This local supersaturation is necessary as it results in the formation of nuclei of the intermediate cupric hydroxide, $Cu(OH)_2$, phase.[45] $Cu(OH)_2$ is comprised of $[Cu(OH)_6]^{4-}$ octahedra that are stabilised at low temperatures through hydrogen bonds.[46] By simply raising the temperature, these hydrogen bonds can be broken, typically resulting in the rapid growth of copper (II) oxide nanostructures.

In order to form the copper (I) oxide structures in the present work, glucose (a "reducing sugar") was added to the synthesis. It has been reported many times that copper-citrate complexes (*i.e.* Benedict's solution) or copper-tartrate complexes (*i.e.* Fehling's solution) can be reduced by glucose to give rise to brick red Cu_2O precipitates, and so these reactions are commonly applied in the analytical determination of saccharides.[28,47] This role of glucose as a reductant in the present work was also verified experimentally. It was found that when the sugar was removed from the synthetic mixture, and the resulting crystals analysed via XRD, aggregates of CuO were revealed rather than 8-branched Cu_2O. It is interesting to see that the morphology of the CuO particles appears to be aggregates of small nanocrystallites rather than regularly shaped monocrystalline polyhedrons (**Figure S4** in SI).

The appearance of the Cu metal phase in the PXRD pattern of the 13 h sample (**Figure 2c**) is simply the result of a further reduction from the Cu^{2+} ions to Cu^{+} and then to Cu. Feng *et al*. reported the synthesis of Cu_2O octahedral crystals and observed weak diffraction peaks of the Cu (111) and (211) planes alongside the expected Cu_2O diffraction peaks.[48] The reason was that the reducing agent used was twice the amount of the stoichiometric ratio required to reduce the Cu^{2+} to Cu^{+}, and so some Cu^{+} was further reduced to Cu. The same was the case in the present work due to the nature of glucose, which exists as three isomers: two cyclic and one linear. It is the aldehyde group on the linear chain that can be oxidised to form a carboxylic acid group and so as more of the linear form of glucose was oxidised, more was produced from the cyclic forms in the solution according to Le Chatelier's principle.[49] This means that, when the amount of glucose used is in excess, it is able to continue to reduce copper from Cu^{2+} to Cu^{+} and, eventually, to Cu. Due to the large difference between the 1st ionisation energy (745.5 kJ/mol) and the 2nd ionisation energy (1957.9 kJ/mol) of copper, the reduction of Cu^{+} would start when most Cu^{2+} have already been reduced to Cu^{+}. Indeed, in the present work, Cu only appeared after a long time reaction, *i.e*. 13 h. When the reaction was allowed to continue for a much longer period of 20 days, the main phase detected via XRD analysis had become Cu and only two very low intensity Cu_2O peaks could be detected. (**Figure S5** in SI).

The reduction from Cu^{2+} to Cu^{+} did not take place in the solution but actually on the surface of the growing crystal or the $Cu(OH)_2$ nuclei as Cu^{+} is unstable in water and rapidly undergoes a disproportionation reaction when added to aqueous media. This reaction is exothermic with a standard electrode potential, $E^{\emptyset}$, of + 0.37 V and so will occur spontaneously.[50] It can be concluded, therefore, that some copper/polymer cations, Cu^{2+}/PVP, in the solution would aggregate into large disordered particles with some anions to balance the charge. The reduction of the cations occurs only inside these aggregates, resulting in Cu_2O seed crystals.

In order for the branch growth to occur so rapidly on the {111} surfaces, the precursor must have a strong attraction to the central Cu_2O seed crystal surface. This leads to the interesting possibility that the {111} faces of the seed crystal may have an overall negative surface charge, causing the branch growth to occur so rapidly along the <111> zone axes.

In aqueous solution, exposed metal ions on crystal surfaces are typically covered with hydroxyl (OH^{-}) groups, with the extent of the coverage dependent on the pH value of the solution. At low, acidic pH values, these OH groups will not be stable. The addition of the buffer solution in the present work meant the pH remained neutral and so the terminating OH groups remain stable. Studies of the terminating facets of metal oxide surfaces and models of their electronic structures have revealed that the charge on the terminating hydroxyl groups is highly dependent on the specific electronic structure of the related crystal plane,[51-53] *i.e*. it is dependent on the number of metal ions that the OH^{-} group is coordinated to.

In the Cu_2O crystal lattice, each Cu^{+} ion is doubly coordinated, *i.e*. it is connected to two neighbouring O^{2-} ions. This means that it donates a charge of +½ per bond, and so Cu^{+} cation on a Cu_2O crystal surface will donate +½ charge to any OH^{-} group it is coordinated to. Therefore, if a hydroxyl group is doubly coordinated (connected to two Cu^{+} cations) as shown in middle of **Figure 4**; the overall charge of the site is neutral. If a hydroxyl group is singly coordinated, however, the overall charge of the site would become negative $(Cu–OH)^{0.5–}$ (right model of **Figure 4**). Conversely, if the hydroxyl group is triply coordinated then the overall charge of the site would become positive $[(Cu–)_3OH]^{0.5+}$(left model of Figure 4).

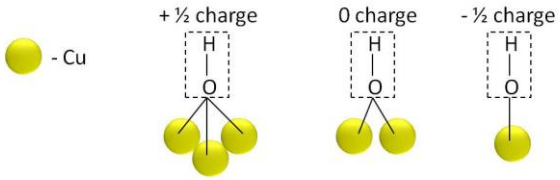

Figure 4. Illustration of the charges of terminating hydroxyl groups when they are triply, doubly or singly coordinated with Cu^{+} cations from the Cu_2O crystal surface.

When the terminal facets along the principal axes of Cu_2O were studied, it could be determined that each face had differently coordinated OH groups. **Figure S6** in SI shows the structure of the (100) surface where it can be seen that only doubly coordinated terminating oxygen atoms are present and so all the hydroxyl sites on the (100) surface would be neutral. **Figure S7** in SI shows the structure of the (110) surface. In this case, the surface oxygen atoms are all connected to three Cu ions (one in the surface layer and two in a lower layer). This means that the terminating hydroxyl groups on the (110) surface would all be triply coordinated and, therefore, positively charged $[(Cu–)_3OH]^{0.5+}$ sites are present.

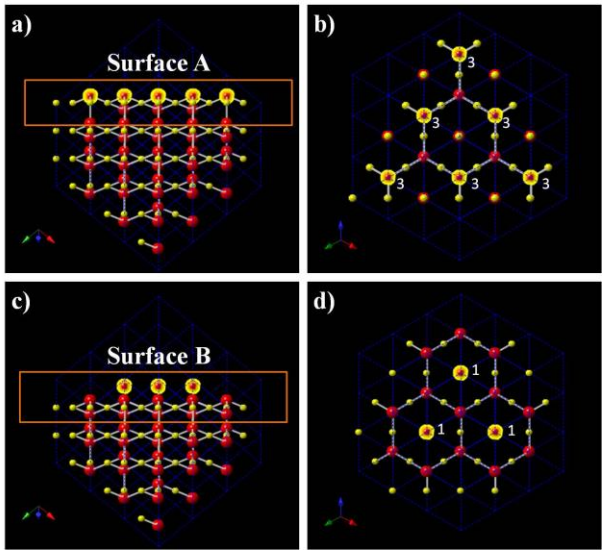

Figure 5. Model of the Cu_2O structure where red spheres represent O and yellow spheres represent Cu. The surface atoms are highlighted. a) A profile view of the (111) facet showing one of the possible terminating surfaces, labelled Surface A. b) Image with the view direction down the (111) terminating plane, Surface A, showing only those atoms from within the orange rectangle marked in a). In Surface A, each surface O is connected to three Cu and so they have been labelled '3'. The highlighted Cu atoms exist on the surface and are not fully coordinated within the crystal structure. c) A profile view of the (111) facet showing the other possible terminating surface, labelled Surface B. d) Image with the view direction down the (111) terminating plane, Surface B, showing only those atoms from within the orange rectangle marked in c). In Surface B, each

surface O is connected to only one Cu (directly underneath) and so they have been labelled '1'.

The situation becomes more complex when the terminating (111) facet is studied as it is comprised of layers of alternating triply and singly coordinated oxygen sites, and so the surface charge depends on which point the structure is stopped at. **Figure 5** displays the two possible terminating faces, which have been labelled Surface A (with triply coordinated hydroxyl groups) and Surface B (with singly coordinated hydroxyl groups). Surface B is the only terminating surface to exist with a negative charge and so the only viable candidate for a strong attraction with the positive Cu^{2+}/PVP precursor. Surface A, however, would have the opposite effect and so it must be considered which possible terminating {111} surface is most likely to be the true one.

For this purpose, it is necessary to study the Cu atoms in the surface layers. In Surface B all of the Cu atoms are fully coordinated within the structure, *i.e.* they are already connected to two O atoms. In Surface A, however, some of the Cu atoms are not fully coordinated and are only connected to one O atom (as highlighted in **Figure 5b**). Surface A would, therefore, be highly unstable as additional oxygen would rapidly be added to the structure to ensure the exposed Cu cations were fully coordinated. As soon as all of the singly coordinated Cu ions in Surface A have been fully coordinated, the terminating plane once again becomes the much more favourable Surface B. The most stable terminating (111) face will, therefore, be Surface B and so will exhibit a negative charge.

This negative charge, unique to the {111} terminating facets explains why branch growth happens so rapidly only along the <111> zone axes, due to a fast deposition of Cu^{2+}/PVP clusters followed by a reduction of Cu^{2+}, causing a deviation from classical crystal growth and resulting in the 8-branched Cu_2O structure.

It is well known that the favourable final morphology of a crystal is the equilibrium shape that results from minimizing the surface free energy, as first suggested by Curie and Wulff over a century ago.[54,55] The typical morphologies of Cu_2O crystals are cubic (formed by 6 {100} facets), octahedral (consisting of 8 {111} facets), and rhombic dodecahedral (composed by 12 {110} facets).[56] If only thermodynamic factors are considered, the latter should be the most stable morphology (with the minimum surface energy), since the {110} planes give the largest *d*-spacing (**Figure 2**). In the present work, however, the morphology formation of Cu_2O crystals is governed by both kinetic (at early stage) and thermodynamic (at late stage) factors. The {111} faces grow out due to the fast growth rate. The growth of the 8-branched particles pre-established the 8 corners of a cube, followed by further growth filling in the gap between the branches, leading to the formation of the cubic morphology.

As the crystallites grow larger there must also be a movement of PVP out of the structure over time, as supported by the TGA results (**Figure S3** in SI), *i.e.* the ratio of PVP to Cu free in solution must increase as the Cu^{+} are absorbed into the growing crystals. Xu *et al*. [30] studied the growth of different Cu_2O morphologies using EDTA salt as both the chelating reagent and reductant and observed that the ratio of EDTA to Cu^{2+} in solution affected the growth direction in a similar way to the present work. When the EDTA:Cu^{2+} ratio was 1, the prominent growth direction was along the <111> zone axes but when the EDTA:Cu^{2+} ratio was 2, the <100> directions became the prominent growth routes and so a cubic morphology was observed. The authors attribute this solely to the ability of the EDTA to stabilise the {100} surfaces, hence the cubic morphology, but this fails to explain why the branching along the <111> directions happens so rapidly during the initial stage and also assumes that the branches are single crystalline from the earliest growth stage which has been proven not to be the case by the HRTEM results obtained during the present work (**Figures 3c** and **3d**).

Combining observations from the present work with those from published studies, it is now much more clear that it is both the existence of the Cu^{2+}/PVP clusters and the unique electronic structure of the terminating {111} planes that causes the rapid branch growth along the <111> zone axes. Over time, as the ratio of organic to Cu cations increases, the amount of Cu^{2+}/PVP clusters in the solution will decrease and so the role of the organic as a stabiliser for the {100} facets starts to become more prominent than its role as an agent for Cu^{2+} aggregation along the <111> directions. This mechanism explains both the initial rapid growth along <111>, the subsequent slowing of growth in these directions and, instead, a transition from an 8-branched to a cubic morphology.

Summary of Growth Mechanism

It is now possible to propose a new, non-classical growth mechanism for the 8-branched Cu_2O structures. Initially, Cu^{2+} ions coordinate with the lone electron pairs on N and O atoms in the long, linear PVP molecules, forming many clusters of a positively charged Cu^{2+}/PVP matrix. A buffer solution is then added, which maintains the pH at 7 and causes supersaturation of the Cu^{2+} ions in these clusters, forming nuclei of the intermediate phase, $Cu(OH)_2$. The $Cu(OH)_2$ nuclei, which most likely exist with an octahedral shape,[45,46] are reduced upon heating with the reducing sugar, glucose, giving rise to Cu_2O seed crystals.

The positively charged Cu^{2+}/PVP precursor clusters are attracted to the negative hydroxyl groups which exist only on the {111} Cu_2O terminating facets (**Figure 6a**). This results in rapid aggregation of linear Cu^{2+}/PVP chains along the <111> directions, leading to the 8-branched structures observed at the short growth time of 1.5 h (**Figure 6b**). The Cu^{+} ions within the branches are able to gather closely together and undergo recrystallization upon reduction to form many nanocrystallites of Cu_2O.

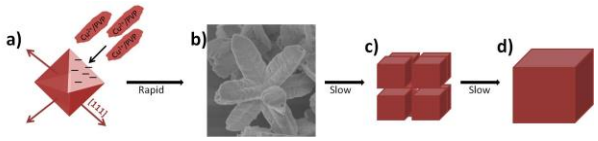

Figure 6. Illustration of the growth of 8-branched Cu_2O structures followed by their transition to a cubic morphology. a) Positively charged Cu^{2+}/PVP clusters are attracted to the negatively charged terminating hydroxyl groups on the {111} facets of Cu_2O seed crystals resulting in rapid aggregation along the <111> directions. b) The earliest appearance of the 8-branched structure where disordered branches grow out from a central seed crystal. c) The branches move towards a cubic shape as the Cu_2O nanocrystallites within them grow larger, self-orientated, and join together. d) Finally the branches grow large enough to join together, forming a perfect cubic morphology.

As the reaction time increases, the Cu_2O nanocrystallites embedded in the branches grow larger, self-orientate, and join together. According to the drive to minimize the surface free energy of the crystals, the gaps between the branches are filled gradually and the particle morphology changes towards a cubic shape as the reaction proceeds, reflecting the cubic unit cell of Cu_2O (**Figure 6c**). This means that, after the initial rapid growth along the <111> directions, there is then predominant growth on the {100} facets. Eventually, the branches grow large enough that they are able to join together, forming the perfect cubic morphology that is observed after a reaction time of 13 h (**Figure 6d**). The cubic shape is the thermodynamically favoured morphology. Consequently, the growth of branches along the <111> direction is kinetically controlled, while the formation of cubes is thermodynamically controlled.

CONCLUSIONS

Whilst there have been previous reports of the range of morphologies Cu_2O crystals can adopt, there have still been many questions left unanswered in the discussions about how and why these morphologies have originated. Some have reported that the formation of 8-branched Cu_2O structures followed by a transition to a cubic morphology is simply a result of faster growth along the <111> directions.[28] Others have suggested preferential growth on different facets is due to the pH of the initial solution [31,48] or of the presence of organic materials which may stabilize certain faces.[30] All of these studies, however, make the assumption that the branches are single crystalline at all growth stages and so, after the initial nucleation and formation of a central seed crystal, the branches still grow epitaxially via the classical "bottom-up" route.

Through HRTEM and SAED analysis, however, it has been shown that this cannot be the case due to the polycrystalline nature of the branches at early stages and to the existence of an organic matrix in the branches from which nanocrystallites of Cu_2O are formed. This work, therefore, challenges conventional knowledge and the classical theories and instead shows that the formation of a Cu^{2+}/PVP matrix in the solution competes with the classical crystal growth process, leading to aggregation of PVP and Cu cations followed by crystallization to Cu_2O within the organic matrix.

The aggregation of precursor molecules/ions before the development of individual free crystals has been observed in many synthetic systems. Such an aggregation often forms large spherical particles and leads to a reversed crystal growth route, *i.e*. crystallisation takes place on the particles' surface followed by an extension from the surface to the core.[57,58] In the present work, however, the highly selective deposition of Cu^{2+}/PVP clusters on specific facets results in an 8-branched morphology rather than spherical particles. Consequently, reversed crystal growth is not observed.

Nevertheless, the surface charge driven mechanism is another type of non-classical crystal growth route. Studies of the electronic structure of the principal terminating facets of Cu_2O demonstrate differently charged hydroxyl groups on the different terminating facets, which play a key role in the rapid branch formation. This mechanism, whereby charged surface hydroxyl groups attract precursor molecules/ions, has also been found to be the case recently for snowflake-like hematite crystals, with six-fold symmetry, which display rapid branch growth along the $<11\bar{2}0>$ directions.[59] In that process, the $\{11\bar{2}0\}$ faces were shown to contain positively charged hydroxyl sites, which were able to attract $[Fe(CN)_6]^{3-}$ anions.

It is vital to fully understand the mechanism by which crystals such as these form as only by developing a true understanding of their growth can we then stop the formation process at desired points and alter the morphology if required, tailoring the desired properties of these crystals for their various applications.

SUPPORTING INFORMATION

More SEM images, TGA results, XRD patterns and crystal surface structures are supplied as Supporting Information. This material is available free of charge via the Internet at http://pubs.acs.org.

AUTHOR INFORMATION

Corresponding Author
E-mail: wzhou@st-andrews.ac.uk

ACKNOWLEDGEMENTS

KS would like to thank the University of St Andrews for the studentship, Mr Chang-Yang Chiang for his assistance with using the CrystalMaker software and Dr Heather Greer for her help with using the TEM microscope. WZZ thanks EPSRC for the financial support to purchase the FEG SEM (EP/F019580/1).

REFERENCES

(1) Grozdanov, I. Electroless Chemical Deposition Technique for Cu_2O Thin Films. *Mater. Lett*. **1994**, *19*, 281–285.

(2) Shen, M. Y.; Yokouchi, T.; Koyama, S.; Goto, T. Dynamics Associated with Bose-Einstein Statistics of Orthoexcitons Generated by Resonant Excitations in Cuprous Oxide. *Phys. Rev. B* **1997**, *56*, 13066–13072.

(3) Xiong, L. B.; Huang, S.; Yang, X.; Qiu, M. Q.; Chen, Z. H.; Yu, Y. p-Type and n-type Cu_2O Semiconductor Thin Films: Controllable Preparation by Simple Solvothermal Method and Photoelectrochemical Properties. *Electrochim. Acta* **2011**, *56*, 2735–2739.

(4) Ma, L. L.; Lin, Y. L.; Wang, Y.; Li, J. L.; Wang, E.; Qiu, M. Q.; Yu, Y. Aligned 2-D Nanosheet Cu(2)O Film: Oriented Deposition on Cu Foil and Its Photoelectrochemical Property. *J. Phys. Chem. C* **2008**, *112*, 18916–18922.

(5) Rakhshani, A. E. Poreparation, Characteristics and Photovoltaic Properties of Cuprous-Oxide - A Review. *Solid State Electron*. **1986**, *29*, 7–17.

(6) Ramirez-Ortiza, J.; Ogura, T.; Medina-Valtierra, J.; Acosta-Ortiz, S. E.; Bosch, P.; de los Reyes, J. A.; Lara, V. H. A Catalytic Application of Cu_2O and CuO Films Deposited Over Fiberglass. *Appl. Surf. Sci*. **2001**, *174*, 177–184.

(7) Yang, H. M.; Ouyang, J.; Tang, A. D.; Xiao, Y.; Li, X. W.; Dong, X. D.; Yu, Y. M. Electrochemical Synthesis and Photocatalytic Property of Cuprous Oxide Nanoparticles. *Mater. Res. Bull*. **2006**, *41*, 1310–1318.

(8) Shishiyanu, S. T.; Shishiyanu, T. S.; Lupan, O. I. Novel NO_2 Gas Sensor Based on Cuprous Oxide Thin Films. *Sens. Actuators B* **2006**, *113*, 468–476.

(9) Mittiga, A.; Salza, E.; Sarto, F.; Tucci, M.; Vasanthi, R. Heterojunction Solar Cell with 2% Efficiency Based on a Cu_2O Substrate. *Appl. Phys. Lett*. **2006**, *88*, 163502.

(10) Briskman, R. N. A Study of Electrodeposited Cuprous-Oxide Photovoltaic Cells. *Sol. Energy Mater. Sol. Cells* **1992**, *27*, 361–368.

(11) Olsen, L. C.; Addis, F. W.; Miller, W. Experimental and Theoretical-Studies of Cu_2O Solar Cells. *Sol. Cells* **1982**, *7*, 247–279.

(12) Snoke, D. Spontaneous Bose Coherence of Excitons and Polaritons. *Science*, **2002**, *298*, 1368–1372.

(13) Zang, Z. G.; Nakamura, A.; Temmyo, J. Single Cuprous Oxide Films Synthesized by Radical Oxidation at Low Temperature for PV Application. *Opt. Express* **2013**, *21*, 11448–11456.

(14) Shahmiri, M.; Ibrahim, N. A.; Shayesteh, F.; Asim, N.; Motallebi, N. Preparation of PVP-coated Copper Oxide Nanosheets as Antibacterial and Antifungal Agents. *J. Mater. Res*. **2013**, *28*, 3109–3118.

(15) Chen, Y.-S.; Liao, C.-H.; Chueh, Y.-L.; Lai, C.-C.; Chen, L.-Y.; Chu, A.-K.; Kuo, C.-T.; Wang, H.-C. High Performance Cu_2O/ZnO Core-shell Nanorod Arrays Synthesized Using a Nanoimprint GaN Template by the Hydrothermal Growth Technique. *Opt. Mater. Express* **2014**, *4*, 1473–1483.

(16) Guo, H.; Liu, L. X.; Li, T. T.; Chen, W. W.; Liu, J. J.; Guo, Y. Y.; Guo, Y. C. Accurate Hierarchical Control of Hollow Crossed $NiCo_2O_4$ nanocubes for superior lithium storage. *Nanoscale* **2014**, *6*, 5491–5497.

(17) Khan, R.; Vaseem, M.; Jang, L.-W.; Yun, J.-H.; Hahn, Y.-B.; Lee, I.-H. Low Temperature Preparation of CuO Nanospheres and Urchin-shaped Structures via Hydrothermal Route. *J. Alloy. Compd.* **2014**, *609*, 211–214.

(18) Gou, L. F.; Murphy, C. J. Solution-phase Synthesis of Cu_2O Nanocubes. *Nano. Lett.* **2003**, *3*, 231–234.

(19) Feng, L. L.; Zhang, C. L.; Gao, G.; Cui, D. X. Facile Synthesis of Hollow Cu_2O Octahedral and Spherical Nanocrystals and Their Morphology-dependent Photocatalytic Properties. *Nanoscale Res. Lett.* **2012**, *7*, 276.

(20) Lu, C.; Qi, L.; Yang, J.; Wang, X.; Zhang, D.; Xie, J.; Ma, J. One-pot Synthesis of Octahedral Cu_2O Nanocages via a Catalytic Solution Route. *Adv. Mater.* **2005**, *17*, 2562–2567.

(21) Chen, K. F.; Sun, C. T.; Song, S. Y.; Xue, D. F. Polymorphic Crystallization of Cu_2O Compound. *CrystEngComm* **2014**, *16*, 5257–5267.

(22) Siegfried, M. J.; Choi, K. S. Electrochemical Crystallization of Cuprous Oxide with Systematic Shape Evolution. *Adv. Mater.* **2004**, *16*, 1743–1746.

(23) Siegfried, M. J.; Choi, K. S. Directing the Architecture of Cuprous Oxide Crystals During Electrochemical Growth. *Angew. Chem. Int. Ed.* **2005**, *44*, 3218–3223.

(24) Siegfried, M. J.; Choi K. S. Elucidating the Effect of Additives on the Growth and Stability of Cu_2O Surfaces via Shape Transformation of Pre-grown Crystals. *J. Am. Chem. Soc.* **2006**, *128*, 10356–10357.

(25) Yao, W.-T.; Yu, S.-H.; Zhou, Y.; Jiang, J.; Wu, Q.-S.; Zhang, L.; Jiang, J. Formation of Uniform CuO Nanorods by Spontaneous Aggregation: Selective Synthesis of CuO, Cu_2O, and Cu Nanoparticles by a Solid-liquid Phase arc Discharge Process. *J. Phys. Chem. B* **2005**, *109*, 14011–14016.

(26) Taneja, P.; Chandra, R.; Banerjee, R.; Ayyub, P. Structure and Properties of Nanocrystalline Ag and Cu_2O Synthesized by High Pressure Sputtering. *Scr. Mater.* **2001**, *44*, 1915–1918.

(27) Kumar, R. V.; Mastai, Y.; Diamant, Y.; Gedanken, A. Sonochemical Synthesis of Amorphous Cu and Nanocrystalline Cu_2O Embedded in a Polyaniline Matrix. *J. Mater. Chem.* **2001**, *11*, 1209–1213.

(28) Wang, D. B.; Mo, M. S.; Yu, D. B.; Xu, L. Q.; Li, F. Q.; Qian, Y. T. Large-scale Growth and Shape Evolution of Cu_2O Cubes. *Cryst. Growth Des.* **2003**, *3*, 717–720.

(29) Ram, S.; Mitra, C. Formation of Stable Cu_2O Nanocrystals in a New Orthorhombic Crystal Structure. *Mater. Sci. Eng. A* **2001**, *304*, 805–809.

(30) Xu, J. S.; Xue, D. F. Five Branching Growth Patterns in the Cubic Crystal System: A Direct Observation of Cuprous Oxide Microcrystals. *Acta Mater.* **2007**, *55*, 2397–2406.

(31) Wang, L.-C.; Jia, H.; Shi, L.-Y.; Liao, N.; Yu, X.-J.; Jin, D.-L. Controlled Synthesis of Cu_2O Micro-crystals with Various Morphologies by Adjusting Solution Conditions. *Inorg. Mater.* **2010**, *46*, 847–851.

(32) Daltin, A.-L.; Addad, A.; Baudart, P.; Chopart, J.-P. Morphology of Magneto-electrodeposited Cu_2O Microcrystals. *CrystEngComm* **2011**, *13*, 3373–3377.

(33) Bravais, A. Études Crystallographiques. *Paris: Gauthier-Villars*, **1866**.

(34) Friedel, M. G. Études sur la loi de Bravais. *Bull. Soc. Fr. Mineral Cristallogr.* **1907**, *30*, 326–455.

(35) Donnay, J. D. H.; Harker, D. A New Law of Crystal Morphology Extending the Law of Bravais. *Am. Mineral.* **1937**, *22*, 446–467.

(36) Hartman, P.; Perdok, W. G. On the Relations Between Structure and Morphology of Crystals. *Acta Cryst.* **1955**, *8*, 521–529.

(37) Greer, H. F.; Zhou, W. Z. Electron Diffraction and HRTEM Imaging of Beam Sensitive Materials, *Crystallography Review*, **2011**, *17*, 163–185.

(38) Mahmoud, M. A.; Tabor, C. E.; El-Sayed, M. A.; Ding, Y.; Wang, Z. L. A New Catalytically Active Colloidal Platinum Nanocatalyst: The Multiarmed Nanostar Single Crystal. *J. Am. Chem. Soc.* **2008**, *130*, 4590–4591.

(39) Lignier, P.; Bellabarba, R.; Tooze, R. P.; Su, Z. X.; Landon, P.; Menard, H.; Zhou, W. Z. Facile Synthesis of Branched Ruthenium Nanocrystals and Their Use in Catalysis. *Cryst. Growth Des.* **2012**, *12*, 939–942.

(40) Deng, H.; Liu, C. M.; Yang, S. H.; Xiao, S.; Zhou, Z.-K.; Wang, Q.-Q. Additive-Mediated Splitting of Lanthanide Orthovanadate Nanocrystals in Water: Morphological Evolution from Rods to Sheaves and to Spherulites. *Cryst. Growth Des.* **2008**, *8*, 4432–4439.

(41) Greer, H. F.; Liu, M.-H.; Mou, C.-Y.; Zhou, W. Z. Dipole Field Driven Morphology Evolution in Biomimetic Vaterite. *CrystEngComm* **2016**, *18*, 1585–1599.

(42) Soltani, N.; Saion, E.; Erfani, M.; Rezaee, K.; Bahmanrokh, G.; Drummen, G. P. C.; Bahrami, A.; Hussein, M. Z. Influence of the Polyvinyl Pyrrolidone Concentration on Particle Size and Dispersion of ZnS Nanoparticles Synthesized by Microwave Irradiation. *Int. J. Mol. Sci.* **2012**, *13*, 12412–12427.

(43) Harada, T.; Fujiwara, H. Formation of Rod Shape Secondary Aggregation of Copper Nanoparticles in Aqueous Solution of Sodium Borohydride with Stabilizing Polymer. *J. Phys. Conf. Ser.* **2007**, *61*, 394–398.

(44) Oskam, G. Metal Oxide Nanoparticles: Synthesis, Characterization and Application. *J. Sol-Gel Sci. Technol.* **2006**, *37*, 161–164.

(45) Zhang, Q. B.; Zhang, K. L.; Xu, D. G.; Yang, G. C.; Huang, H.; Nie, F. D.; Liu, C. M.; Yang, S. H. CuO Nanostructures: Synthesis, Characterization, Growth Mechanisms, Fundamental Properties, and Applications. *Prog. Mater. Sci.* **2014**, *60*, 208–337.

(46) Rodriguez-Clemente, R.; Serna, C. J.; Ocana, M.; Matijevic, E. The Relationship of Particle Morphology and Structure of Basic Copper(II) Compounds Obtained by Homogeneous Precipitation. *J. Cryst. Growth* **1994**, *143*, 277–286.

(47) Petrucci, R. H. *General Chemistry*, 4th ed., Macmillan Publishing Company, New York, 1985; p 848.

(48) Feng, L. L.; Zhang, C. L.; Gao, G.; Cui, D. X. Facile Synthesis of Hollow Cu_2O Octahedral and Spherical Nanocrystals and Their Morphology-dependent Photocatalytic Properties. *Nanoscale Res. Lett.* **2012**, *7*, 276.

(49) Le Chatelier, H.; Boudouard, O. Limits of Flammability of Gaseous Mixtures. *Bull. Soc. Chim. Fr.* **1898**, *19*, 483–488.

(50) MacKay, K. M.; MacKay, R. A.; Henderson, W. *Introduction to Modern Inorganic Chemistry*, 6th Edition, Nelson Thornes Ltd., Cheltenham, **2002**; p 347.

(51) Cornell, R. M.; Schwertman, U. *The Iron Oxides: Stucture, Properties, Reaction, Occurences and Use*. Second Edition, Wiley VCH GmbH&Co. **2003**.

(52) Rochester, C. H.; Topham, S. A. Infrared Study of Surface Hydroxyl-groups on Hematite. *J. Chem. Soc. Faraday Trans.* 1, **1979**, *75*, 1073–1088.

(53) Barron, V.; Torrent, J. Surface Hydroxyl Configuration of Various Crystal Faces of Hematite and Goethite. *J. Colloid Interface Sci.* **1996**, *177*, 407–410.

(54) Curie, P. On the Formation of Crystals and on the Capillary Constants of Their Different Faces. *Bull. Soc. Fr. Mineral Cristallogr.* **1885**, *8*, 145–150.

(55) Wulff, G. On the Question of Speed of Growth and Dissolution of Crystal Surfaces. *Z. Kristallogr.* **1901**, *34*, 449–530.

(56) Qin, B.; Zhao, Y. B.; Li, H.; Qiu, L.; Fan, Z. Facet-dependent Performance of Cu_2O Nanocrystal for Photocatalytic Reduction of Cr(VI). *Chinese J. Catal.* **2015**, *36*, 1321–1325.

(57) Yao, J. F.; Li, D.; Zhang, X. Y.; Kong, C. H.; Yue, W. B.; Zhou, W. Z.; Wang, H. T. Cubes of Zeolite A with an Amorphous Core. *Angew. Chem. Int. Ed.* **2008**, *47*, 8397–8399.

(58) Zhou, W. Z. Reversed Crystal Growth: Implications for Crystal Engineering. *Adv. Mater.* **2010**, *22*, 3086–3092.

(59) Liu, Z.; Chiang, C.-Y.; Li, W.; Zhou, W. Z. The Role of Surface Hydrolysis of Ferricyanide Anions in Crystal Growth of Snowflake-shaped Alpha-Fe_2O_3. *Chem. Commun*. **2015**, *51*, 9350–9353.

For Table of Contents Use Only (TOC)

Surface Charge Driven Growth of Eight-Branched Cu_2O Crystals

Katherine Self and Wuzong Zhou

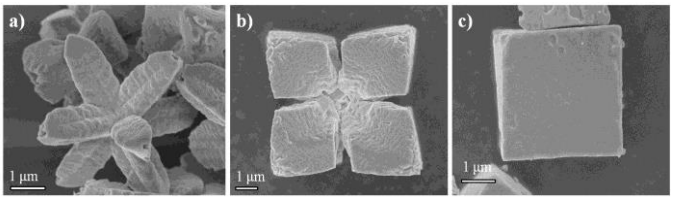

Synopsis: 8-branched Cu_2O crystals that undergo a transition to a cubic shape over time are synthesised. The formation of Cu^{2+}/PVP clusters is shown to play a key role in the reduction of Cu^{2+}, nucleation of Cu_2O crystals and rapid growth of branches along all eight <111> directions of cubic Cu_2O, due to negatively charged hydroxyl sites on the {111} surfaces.